

www.acsaem.org Article

Visible Light-Assisted Charge Extraction in High-Band-Gap SrTiO₃ through the Integration of a Triplet Sensitizer-Emitter Thin Film

Kelvin V. Y. Jie, M. Fairus Ahmad, * A. Rahman Mohmad, A. Mawardi Ismail, M. Natashah Norizan, M. Mahyiddin Ramli, Safizan Shaari, Yusran Sulaiman, Shamsul A. A. Rais, and Shazlina Johari



Cite This: ACS Appl. Energy Mater. 2024, 7, 799-809



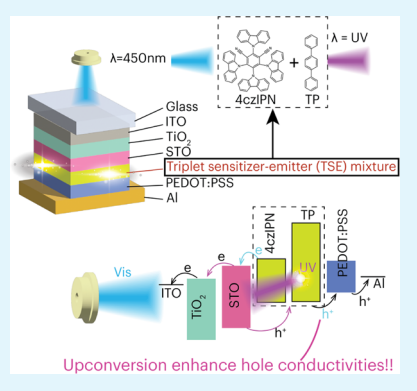
ACCESS I

Metrics & More

Article Recommendations

Supporting Information

ABSTRACT: A challenge in PV designs, including those with an electron transport layer (ETL), is the presence of 'parasitic absorbers'. These are layers that absorb light without significantly converting it to electrical current, impacting the total external quantum efficiency (EQE). Strontium titanate (STO), a high-band-gap (3.20 eV) perovskite metal oxide, holds promise as an electron transport layer (ETL) for solar energy harvesting. Despite STO's potential, it primarily operates in the UV spectrum, not fully utilizing the broader light range, and hence can be the source of parasitic absorbers. In this study, we report a significant enhancement in the EQE of STO through the integration of a triplet sensitizer-emitter (TSE) system, designed to upconvert the visible spectrum into UV light and improve the charge extraction from STO. The TSE system uses carbazolyl dicyanobenzene (4CzIPN) as a sensitizer and p-terphenyl (TP) as an emitter. To investigate the EQE of such a system, we fabricate STO as a PV cell. The revised PV cell architecture (ITO/TiO2/STO/TSE/PEDOT:PSS/Al) is a modification of the conven-



tional configurations (ITO/TiO2/STO/PEDOT:PSS/Al). With the TSE thin film, the modified STO PV cell shows better charge extraction under sunlight compared to the standard STO PV cell, indicating that the upconversion process can enhance the hole conductions from STO to PEDOT:PSS through the TSE system. We noted an EQE increase with intense light of $\lambda > 345$ nm in thicker TSE layers and a decrease in the EQE under similar light intensity in thinner TSE layers. The Kelvin probe force measurement (KPFM) data showed that the TSE layer receives holes from STO under illumination. Additionally, time-resolved photoluminescence (TRPL) experiments showed that the TSE/STO thin film is able to produce UV emission after irradiation with lower energy light. Then, the EQE variation in thicker TSE layers under intense irradiation can be attributed to the solid-state upconversion, indicating its thickness-dependent performance. These findings underline the strategies for maximizing the utilization of the solar spectrum in PV applications.

KEYWORDS: triplet-triplet annihilation, photon upconversion, perovskite, scanning Kelvin probe microscopy, photovoltaic, renewable energy

INTRODUCTION

Photovoltaic (PV) technology has attracted much interest as a potential approach for generating sustainable energy due to the increased global awareness of the requirement for carbonneutral energy production for environmental sustainability. As compared with other renewable energy sources and fossil-based conventional energy sources, solar energy is rather abundant, delivering several kilowatt-hours per square meter daily. Among many PV technologies, the perovskite-based PV technology has received much attention due to its large band gap for utilizing higher energy photons for energy conversion and generating a higher open-circuit voltage (VOC).^{3–5}

To enhance the efficiency of photovoltaic systems, technologies such as luminescent solar concentrators⁶ and multijunction cell technology⁷ are used. These technologies help the system capture and utilize a broader range of light from the spectrum. The inverted solar cell design also refines this process. It provides stability and is compatible with a variety of materials, including metal oxides. Furthermore, the electron transport layer $(ETL)^{8-10}$ and hole transport layer $(HTL)^{11-15}$ are utilized to facilitate efficient charge separation and transport, reducing the likelihood of charge recombination. Metal oxides, including those used in perovskite solar cells, are commonly employed as ETLs.8 However, in a photovoltaic structure, some layers like the ETL can act as 'parasitic absorbers'. This means that they might absorb some of the incoming light without contributing much to the generation of electrical current. 16,17 While metal oxides primarily absorb light in the UV region, it is still important to consider their quantum efficiency. This metric

Received: November 27, 2023 Revised: December 21, 2023 Accepted: December 22, 2023 Published: January 10, 2024





ACS Applied Energy Materials

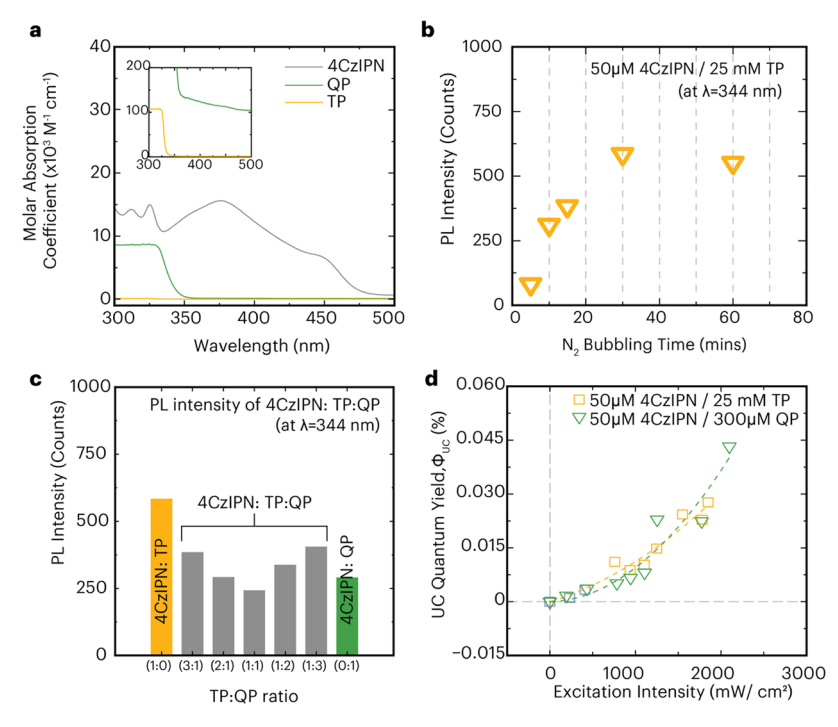


Figure 1. (a) Molar absorption coefficient of 4CzIPN, QP, and TP in benzene. (b) PL intensity at 344 nm of 50 μ M 4CzIPN (1 mL) coupled with 25 mM TP (1 mL) after different N₂ bubbling times (5, 10, 15, 30, and 60 min) under the 450 nm light excitation intensity of 2005 mW cm⁻². (c) PL intensity at 344 nm of 50 μ M 4CzIPN (1 mL) mixed with 25 mM TP and 300 μ M QP with the TP/QP volume (in mL) ratios of [1:0], [3:1], [1:1], [1:2], [1:3], and [0:1] under the 450 nm light excitation intensity of 2098 mW cm⁻². (d) Plotted graph of the TTA-UC quantum yield at 344 nm of emission intensity for 50 μ M 4CzIPN (1 mL) coupled with 25 mM TP (1 mL) and at 354 nm of emission intensity for 50 μ M 4CzIPN (1 mL) coupled with 300 μ M QP (1 mL). For all PL measurements: the light source is 450 nm LED; volume of solution in the cuvette = 2 mL; and light path length through the cuvette = 10 mm.

indicates how these materials convert absorbed photons into electricity.

Strontium titanate (STO) is a kind of metal oxide having a perovskite crystal structure. STO has shown near 100% quantum efficiency¹⁸ in converting photons to electrons during photocatalytic reactions. 19,20 Furthermore, the devices can also be fabricated in an ambient atmosphere. Due to its large band gap (3.20 eV),²⁰ STO requires higher energy photons (to generate free carriers), specifically from the UV region, which comprises only 7% of the solar spectrum. This means that significant portions of the spectrum, such as the visible and infrared, remain unused. This inability to harness photons with energies below their band gap constrains the energy conversion efficiency of single-junction solar cells to the Shockley-Queisser limit. 21,22 Hence, a trade-off exists between using a wider solar spectrum and having a large open-circuit voltage. This is why STO is not commonly used as a light absorber in traditional planar photovoltaic cells. 23 In planar halide perovskite PVs, STO has been efficiently used as an ETL, proving more effective than TiO₂ nanoparticles in extracting charge from halide perovskites.²⁴ It is important to reduce the parasitic absorption in STO to operate as an efficient ETL. Hence, a new strategy to improve the charge extraction from STO should be considered.

The photon upconversion system application in photovoltaic systems has raised interest as it could utilize the lower photon energy to be converted into higher energy photons for solar–electricity conversion.²⁵ It is encouraging to further improve the photovoltaic system by harvesting the upconverted photons. Triplet—triplet annihilation upconversion (TTA-UC) is a process of consuming two energy photons in sensitizer molecules and converting them into a high energy photon

through emitter molecules by a triplet—triplet energy transfer (TTET) process. ²⁶ By interfacing molecular materials having long-lived triplet excitons and solid crystals, we can engineer new behaviors, potentially revolutionizing fields such as photovoltaics, photodetection, sensing, and optical information processing. ²⁷ Numerous studies have integrated the photon upconversion system to improve the photovoltaic response, in the form of liquid and solid-state layers. ^{19,28–34} Most of these studies have primarily targeted the upconversion in infrared and visible spectra with less emphasis on the UV region.

The energy losses during the donor's intersystem crossing (ISC) process, specifically the singlet-triplet (S_1-T_1) state energy gap ($\Delta E_{\rm ST}$), have a negative impact on the energy gain of the overall TTA-UC system, which was studied by Yanai et al.³⁵ They identified a significant problem that impeded the combination of a sensitizer and an annihilator, as the energy level of the annihilator's T₁ state needed to be lower than that of the sensitizer's T1 state. In that study, a thermally activated delayed fluorescence (TADF) molecule called carbazolyl dicyanobenzene (4CzIPN) was used as the sensitizer. It was coupled with emitters p-quarterphenyl (QP) and p-terphenyl (TP) in a deaerated benzene solvent. The small $\Delta E_{\rm ST}$ value of 4CzIPN (0.083 eV) effectively reduces the energy loss during ISC and expands the range of available annihilators. The 4CzIPN/QP couple exhibited a UV upconverted energy $(\Delta E_{\rm UC})$ value of 0.73 eV (445 to 353 nm) with a quantum yield ($\Phi_{\rm UC}$) of 1.95% and a threshold intensity ($I_{\rm th}$) of 0.8 W cm⁻². Similarly, the 4CzIPN/TP couple displayed a $\Delta E_{\rm UC}$ value of 0.83 eV (445 to 343 nm) with a $\Phi_{\rm UC}$ of 1.4% and a $I_{\rm th}$ of approximately 1.8 W cm⁻².

ACS Applied Energy Materials

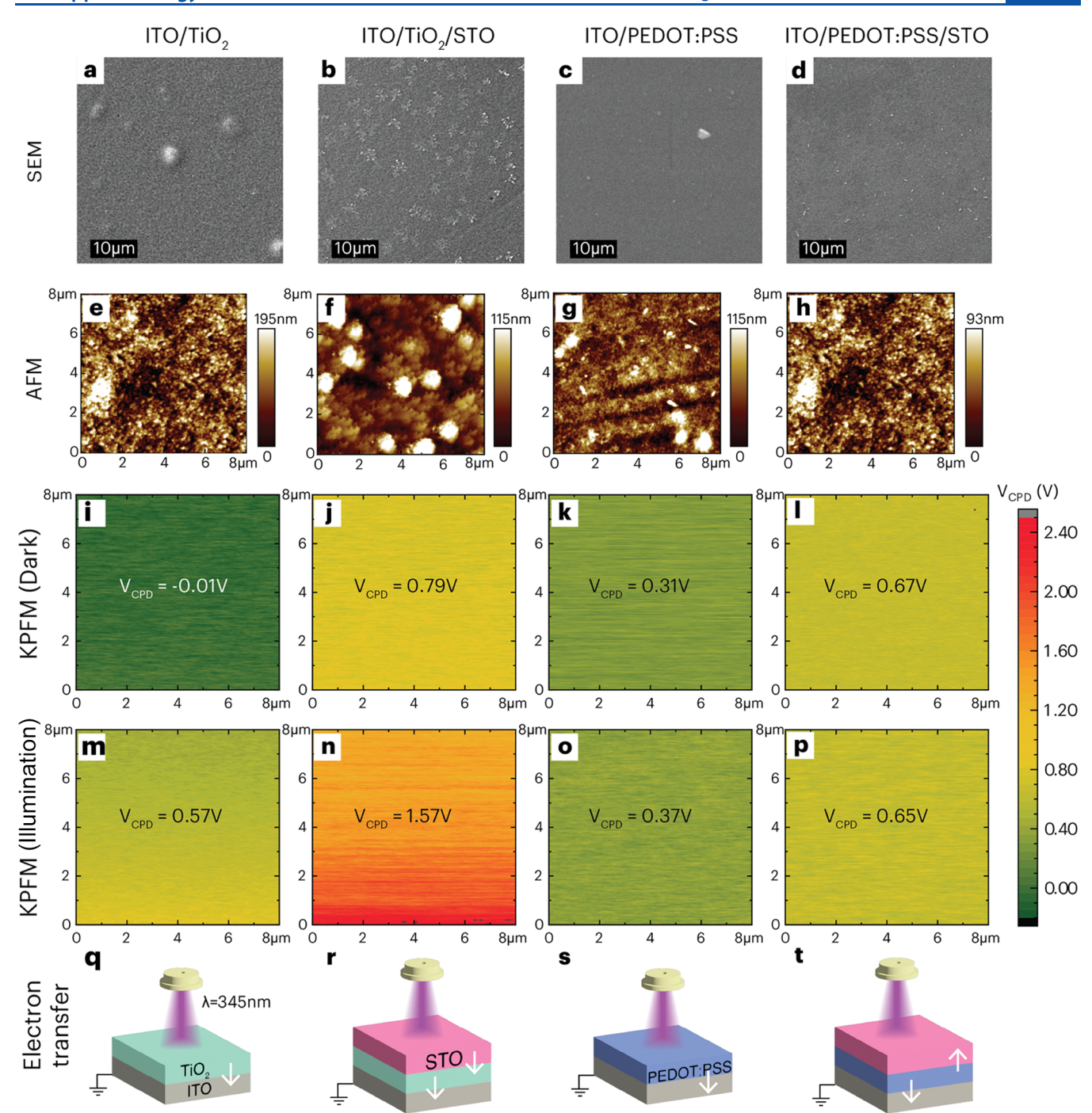


Figure 2. (a-d) SEM morphology images and (e-h) AFM topography images of ITO/TiO_2 , $ITO/TiO_2/STO$, ITO/PEDOT:PSS, and ITO/PEDOT:PSS/STO. Surface potential KPFM images of the same samples under two conditions: (i-l) dark condition and (m-p) illuminated condition of 80 mW m⁻² 345 nm light. (q-t) Summary of electron transfer at the interface after Fermi level alignment under the illuminated condition.

Here, we present and discuss STO as an absorber neighboring with triplet sensitizer—emitter (TSE) molecules to enable the conversion of visible light into UV light for reabsorption by STO. To analyze the quantum efficiency, we fabricated the STO thin film as a photovoltaic cell. We employed the ITO/TiO $_2$ /STO/PEDOT:PSS/Al structure to construct as the conventional STO PV cell. We used TiO $_2$ and PEDOT:PSS to facilitate the conduction of electrons and holes, respectively, to the electrodes. For the TTA-UC process, we used 4CzIPN, TP, and QP molecules. To integrate the TSE system with the STO PV cell, we directly fabricated a TSE layer within the STO PV cell

(referred to as the TSE/STO PV cell). We compared their external quantum efficiency values through the thickness-dependent TSE layer and also the influence of UV and visible light sources.

RESULTS AND DISCUSSION

To identify the emergent properties of the TSE materials, we began by investigating their photoluminescence properties. Figure 1a shows the molar absorption coefficient and ε spectrum of the individual sensitizer (4CzIPN) and the emitters (QP and TP). It shows that 4CzIPN has higher absorbance in the visible

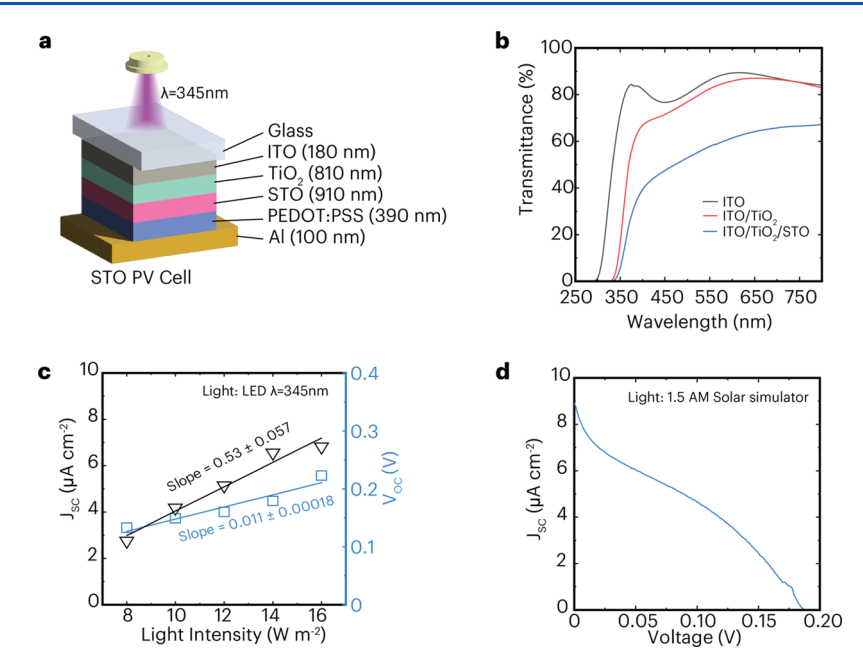


Figure 3. (a) Schematic illustration of the STO PV cell (ITO/TiO₂/STO/PEDOT:PSS/Al) with the thickness measured for each layer. (b) Optical transmittance of ITO, ITO/TiO₂, and ITO/TiO₂/STO. (c) J-V curve of the STO PV cell under irradiance of UV light (λ = 345 nm) with their respective irradiance intensities. (d) J-V curve of the STO PV cell measured under a 1.5 AM solar simulator.

region (from $\lambda \le 480$ nm), followed by QP and TP. QP and TP mostly absorb light in the UV region from $\lambda < 340$ nm.

It is critical to have a high PL intensity from the TTA-UC process, especially in the entire UV region, for light absorption and photogeneration in STO. As shown in Figure S1, the PL spectra of both 4CzIPN/TP and 4CzIPN/QP were measured under $\lambda=450$ nm of excitation light. The spectrum of upconverted photons spanned within 330 < λ < 400 nm, with a peak at $\lambda=344$ nm for 4CzIPN/TP and a double peak ($\lambda=354$ nm & $\lambda=370$ nm) for 4CzIPN/QP. Therefore, for the success of the TTA-UC process, the reabsorption of upconverted light (i.e., UV light) by the unreacted TSE molecules in the surrounding should be avoided.

Dissolved oxygen is known to quench the triplet formation in the TTA-UC process and thus reduce the PL intensity. N_2 bubbling (purging with a flow rate = 10 mL/min) into the TSE pair solution was implemented as a deoxygenation process. Figure 1b shows the PL intensity at $\lambda = 344 \text{ nm}$ after different N_2 bubbling times. The measured PL intensity increased gradually with the N_2 bubbling time until it saturated after 30 min. 30 min of the N_2 purging time appears to be optimum in our setup for reducing a significant amount of dissolved oxygen.

The concentration dependence of the TSE pairs toward the PL intensity was investigated under the irradiation $\lambda=450$ nm. For the case of varying concentrations of 4czIPN (5 to 400 μ M) and fixed concentrations for TP (25 mM) (Figure S2a), it was found that the PL intensity showed an uphill trend (Figure S2b). Suppose two molecules of the sensitizer and two emitter molecules are needed for the TTA-UC process (i.e., a 1:1 mol ratio is needed) but the intensity does not increase further with the 4czIPN concentration after 100 μ M. The uphill trend means that further increase of the sensitizer 4czIPN might induce light reabsorption for the unreacted 4czIPN molecule in the TTA-UC process.

Theoretically, a higher concentration of the emitter molecules could result in a better PL intensity since the quantum yield of a TTA-UC system is limited by the concentration of the annihilator.³⁶ The dependence of the emitter mixture (QP and TP) with different ratios on the PL intensity was studied to find the feasibility of mixed emitter molecules in increasing the PL intensity at λ < 340 nm. 50 μ M 4CzIPN (1 mL) was mixed with 25 mM TP and 300 μ M QP with different TP/QP volume (in mL) ratios of [1:0], [3:1], [2:1], [1:1], [1:2], [1:3], and [0:1]. Figure S3 shows the PL intensity response. The detected upconverted fluorescence peaks at specific wavelengths on the 4CzIPN/TP and 4CzIPN/QP couples are in accordance with the report of ref base-text. 35,37 As shown in Figure 1c, the PL intensity response at $\lambda = 344$ nm was summarized. The highest intensity appeared only for the case of TP/QP = 1:0 (i.e., the 4CzIPN/TP pair). The small intensity cases could be due to the triplet-triplet energy transfer (TTET) mostly happening between 4CzIPN and QP. Additionally, as shown in Figure S3, it was observed that TP/QP = [3:1], [2:1], and [1:1] exhibited a decreasing trend in the photoluminescence intensity of the peak at $\lambda = 370$ nm. In contrast, the original 4CzIPN/QP case consistently showed a higher peak intensity at $\lambda = 370$ nm compared to $\lambda = 354$ nm. This trend suggests that the presence of TP in proximity to QP could induce a redistribution of energy levels in the molecules and a shift in the photoluminescence

Since the 4CzIPN/QP pair could exhibit a strong PL intensity at $\lambda=354$ nm, where STO can partially absorb the light, such a UV light source should also be considered. The UC quantum yield ($\Phi_{\rm UC}$) vs excitation intensity of the 4CzIPN/TP pair (at $\lambda=344$ nm) and the 4CzIPN/QP pair (at $\lambda=354$ nm) was calculated (and is plotted in Figure 1d) using the method as mentioned in the previous study, which is based on the integrated photoluminescence spectral profile of Coumarin 6 (see the Supporting Information). The $\Phi_{\rm UC}$ values obtained for the 4CzIPN/TP and 4CzIPN/QP couples were similar. Their $\Phi_{\rm UC}$ values are different ($\Phi_{\rm UC}$ of 4CzIPN/TP < $\Phi_{\rm UC}$ of 4CzIPN/QP) only in the case of strong light (light intensity > 2000 mW/cm²). The $\Phi_{\rm UC}$ value observed in Figure 1d is lower than that reported in ref 35 (i.e., $\Phi_{\rm UC}\approx 2.4\%$ at 2000 mW/cm²).

ACS Applied Energy Materials

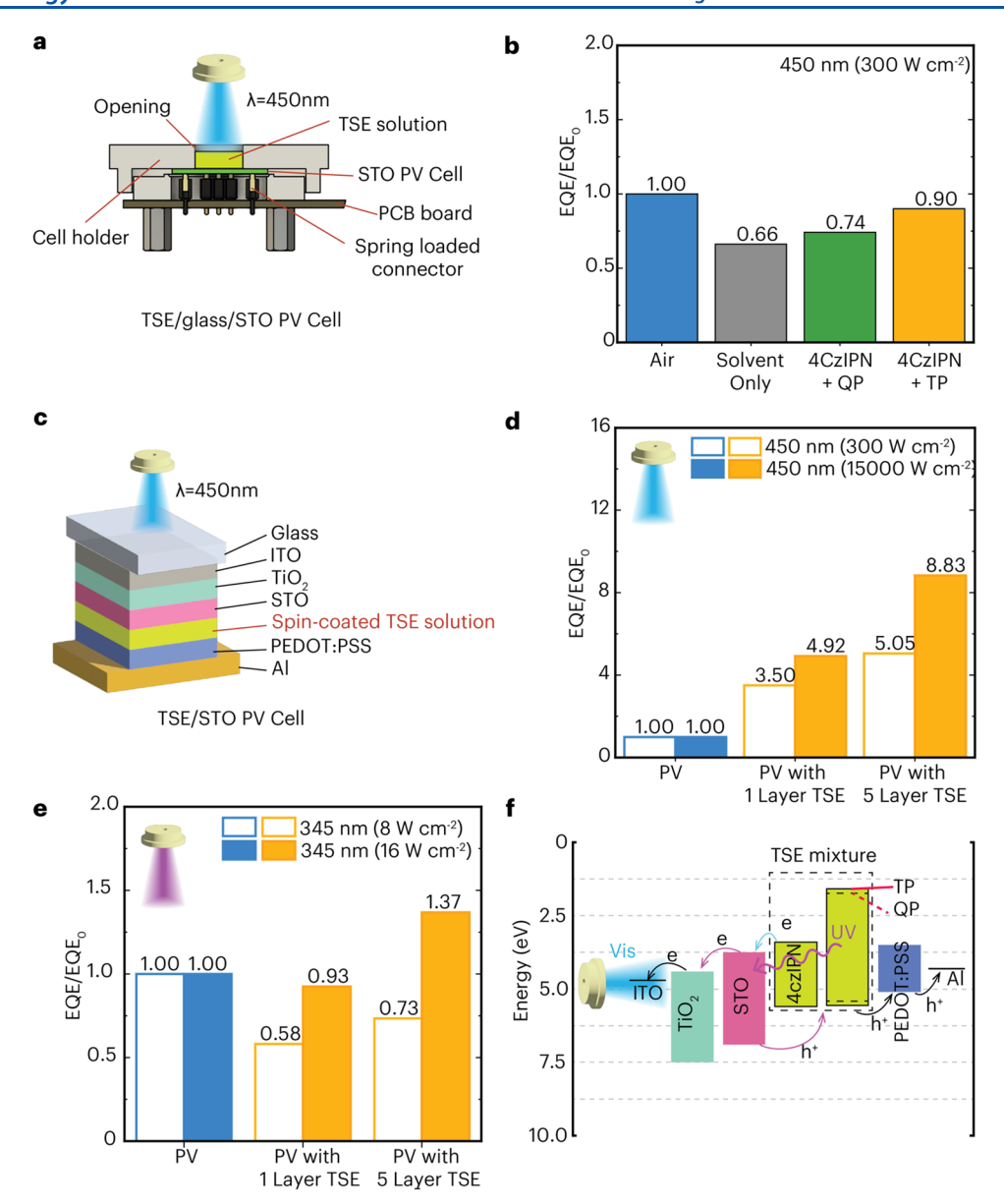


Figure 4. (a) Experimental setup for the I–V characterization of the TSE/glass/STO PV cell using a customized cell holder. (b) EQE/EQE₀ graph of the conventional STO PV cell (air), with benzene only, with 50 μ M 4CzIPN/300 μ M QP solution and with 50 μ M 4CzIPN/25 mM TP solution under 300 W m⁻² (λ = 450 nm) irradiation. (c) Schematic illustration of the TSE/STO PV cell structural design (ITO/TiO₂/STO/TSE/PEDOT:PSS/Al). (d) EQE/EQE₀ graph of the STO PV cell, the STO PV cell with 1 layer of deposited TSE, and the STO PV cell with 5 layers of deposited TSE under 450 nm irradiance with low intensity (300 W m⁻²) and high intensity (15 000 W m⁻²). (e) EQE/EQE₀ graph similar to panel (d) but with UV light irradiation at 8 and 16 W cm⁻². (f) Proposed mechanism of the photogeneration carrier in the TSE/STO thin film PV cell.

This discrepancy can be attributed to the insufficient reduction of oxygen concentration during our N_2 bubbling process. (Note: One of the efficient methods for removing dissolved oxygen is using the repeated freeze–pump–thaw method. Nonetheless, we found that this efficiency level was sufficient to observe the photoresponse effect in our study.

Anatase ${\rm TiO_2}$ and PEDOT:PSS are well-known electron transport layers (ETLs) and hole transport layers (HTLs), respectively. Both types of materials have similar transmittance of light in the UV region. To choose either the inverted or normal structure type of the STO photovoltaic cell, we utilized Kelvin probe force microscopy (KPFM). Figure 2 shows the SEM, AFM, and KPFM images (dark and light conditions) with contact potential difference ($V_{\rm CPD}$) values for ITO/TiO₂, ITO/TiO₂/STO, ITO/PEDOT:PSS, and ITO/PEDOT:PSS/STO.

Based on the SEM images, the coating uniformity of each sample was obtained. The surface roughness of each sample measured by AFM showed a particle size ≤ 100 nm.

 $V_{\rm CPD}$ (contact potential difference) is correlated with work function (Ø), which is described as $V_{\rm CPD} = -(\varnothing_{\rm s} - \varnothing_{\rm t})/q$, where q represents the electron charge and $\varnothing_{\rm s}$ and $\varnothing_{\rm t}$ represent the work functions of the sample and the tip of the cantilever, respectively. A material with a low WF value (a high $V_{\rm CPD}$ value) will donate electrons to a higher WF value (a low $V_{\rm CPD}$ value) caused by the Fermi level alignment. The KFPM measurement was implemented by using a Pt type of cantilever tip (work function of Pt = 5.0 eV) and setting up the ITO surface to be connected to the electrical ground. The cantilever tip was set to 50 nm above the sample. The LED light at $\lambda = 345$ nm was

chosen to represent the upconverted light from the TTA-UC process.

Surface photovoltage (SPV) values could indicate the magnitude of responsiveness of a material toward the irradiation. SPV can be calculated through the difference between the $V_{\rm CPD}$ values under dark (D) and light (L) conditions, i.e., SPV = $V_{\rm CPD,\,L} - V_{\rm CPD,D}$.

Both ITO/TiO₂ and ITO/TiO₂/STO showed positive SPV = +0.58 and +0.78, respectively. These values indicated that under illumination, TiO₂ donated electrons to ITO, and STO donated electrons to TiO₂ (Figure 2q-r). On the other hand, ITO/PEDOT:PSS and ITO/PEDOT:PSS/STO (Figure 2s-t) had a small SPV value (-0.02 < SPV < +0.06). The positive SPV for ITO/PEDOT:PSS means a Fermi level alignment due to the transfer of a photogenerated electron from PEDOT:PSS to ITO, while the negative SPV value in ITO/PEDOT:PSS/STO means PEDOT:PSS receives a photogenerated hole from STO. Overall, due to the high responsiveness in TiO₂ compared to PEDOT:PSS, we considered that the structure of the PV cell should contain TiO₂ as the ETL between STO and ITO.

Figure 3a illustrates the structural design of the STO PV cell (ITO/TiO₂/STO/PEDOT:PSS/Al) along with the measured thickness. The typical optical transmittance result of ITO/ TiO_2/STO is shown in Figure 3b, where light at $\lambda > 350$ nm is partially transmitted. Figure 3c shows the dependency of the short circuit current (J_{SC}) and open-circuit voltage (V_{OC}) of the STO PV cell (ITO/TiO₂/STO/PEDOT:PSS/Al) on the light irradiance intensity under UV light. The STO PV cell exhibited small I_{SC} and V_{OC} , which is typical for a large band gap materialbased PV cell. The fitting slope value showed that the J_{SC} value is more strongly (ca. 50 times) dependent on the light intensity than the $V_{\rm OC}$ value. Even though under the AM 1.5G solar simulator (Figure 3d), the $V_{\rm OC}$ value does not change much. Such saturation of the $V_{\rm OC}$ value could be due to the energetic loss during the quasi-Fermi level splitting between STO and the transport layers, as discussed in a previous study. 41 This brings us to another way to improve the performance of the STO PV cell by increasing the STO layer's light absorbance to generate more photocurrent.

The J_{SC} response for the TSE/Glass/STO PV cell (i.e., TSE/Glass/ITO/TiO₂/STO/PEDOT:PSS/Al) was investigated under λ = 450 nm irradiation. The purpose is to get upconverted light in the UV region from the TSE solution and to be absorbed by STO in the PV cell. As shown in Figure 4a, the PV cell was mounted in a custom solar cell holder, connected to a printed circuit board (PCB) with electrical cathode and anode pin connectors by spring-loaded connectors. The N₂-deoxygenated TSE solution can be dropped on the glass through the cell holder's 1 cm \times 1 cm opening, where the O-ring was used for sealing the liquid. The top of the opening was covered with a glass slide to provide a closed system.

The J_{SC} was recorded and analyzed through the EQE value (i.e., EQE = $(J_{SC}hf)/(I_{in}e)$, where h is the Planck constant, f is the photon frequency, I_{in} is the incident light intensity, and e is the electron charge). The relative EQE (= EQE/EQE₀) gives the ratio of the measured EQE toward the EQE of the conventional STO PV cell. As shown in Figure 4b, the EQE/EQE₀ = 1 is for the STO PV cell, as the glass interfacing with air (i.e., the air/glass/STO PV cell) was used as a control experiment. The influence of benzene solvent on the EQE was also examined for the case of the benzene/glass/STO PV cell. About 34% of the EQE was dropped, which is due to low transmittance of light, probably due to the scattering onto the impurities present in the

solvent or on the surfaces of the glass comprising the device. In the case of the TSE/Glass/STO PV cell, an increase of EQE/EQE0 was observed, indicating that the upconverted light (in the UV region) from the TSE solution increased the photogenerated carriers in the STO PV cell. The EQE/EQE0 of 4CzIPN/TP showed a larger value than that of 4CzIPN/QP, even though their $\Phi_{\rm UC}$ values were similar (Figure 1d), demonstrating that the number of photogenerated carriers in the STO PV cell depends on the absorbance of light at a shorter wavelength ($\lambda \ll 354$ nm). Overall, these data suggest that if we can increase the transmittance of this system, more upconverted photons can be absorbed by STO.

Figure 4c shows the illustration of TSE/STO PV cells (i.e., ITO/TiO₂/STO/TSE/PEDOT:PSS/Al), where the sample was fabricated and investigated for the light responsiveness of the solid/solid interface of TSE and STO in the PV cells. The 4CzIPN/TP pair was chosen due to its higher EQE. The thickness of the TSE film was varied by spin-coating either a single layer or five layers of the TSE solution (4CzIPN/TP in benzene), creating two distinct samples.

Figure 4d shows the EQE/EQE₀ for the conventional PV cell and TSE/STO PV cells with two different thicknesses of the TSE layer under visible light irradiation ($\lambda = 450$ nm). The intensity dependence of the photocurrent response in PV cells was investigated and compared with the data, as shown in Figure 4b. Using the same light intensity of 300 W/cm², the EQE/ EQE₀ value of TSE/STO PV cells was significantly higher compared to that of the conventional PV cell. Furthermore, by transitioning from the TSE/Glass/STO PV cell to the TSE/ STO PV cell, the negative impact related to the light scattering has been eliminated, highlighting the dependence of the TSE upconversion performance on the thickness of the TSE layer. Under 150 times higher intensity (=15 000 W/cm²), the EQE/ EQE₀ value was enhanced further. This result shows that the EQE of TSE/STO PV cells did not saturate (see Figure S4) under the irradiation of a high photon flux, which means that carrier recombination was more suppressed, unlike the conventional STO PV cell. The positive exponential curve of the intensity dependence of the TTA-UC quantum yield relationship (Figure 1d) further supports the increase of the EQE.

To further investigate the sensitization in TSE/STO PV cells, we performed another set of control experiments (Figure S5) with the TP alone on the STO layer (ITO/TiO₂/STO/TP/ PEDOT:PSS/Al), 4CzIPN alone (with varied concentrations) on the STO layer (ITO/TiO₂/STO/4CzIPN/PEDOT:PSS/ Al), and 4CzIPN alone on the TiO_2 layer (ITO/ TiO_2 /4CzIPN/ PEDOT:PSS/Al). Figure S5b shows that the EQE/EQE₀ value of the device with only TP (without the triplet sensitizer 4CzIPN) was relatively smaller compared to the TSE case (Figure S5e). It shows that 450 nm light (i.e., 2.7 eV) is not sufficient to generate charge separation from the large-band-gap TP material (i.e., 3.60 eV) and also STO (i.e., 3.20 eV). When the case of 4CzIPN alone on the STO layer with different amounts of sensitizer was used (Figure S5c for 5 μ M and Figure S5d for 50 μ M), the EQE/EQE₀ value exhibited a concentration dependence relationship. However, the values were not higher than that of PV with STO only (Figure S5a). Moreover, in contrast to TP on STO, 4CzIPN on STO shows a slightly higher photocurrent generation. Those data demonstrate the limited amount of electron conduction in the LUMO of 4CzIPN to the conduction band of STO. Therefore, in the case of TSE on STO, we cannot ignore the possibility of minor carrier (electron) conduction from 4CzIPN to STO, especially near the interface

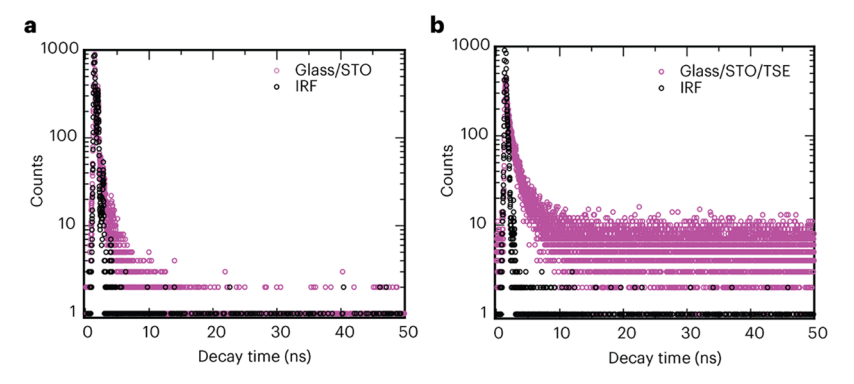


Figure 5. Time-resolved photoluminescence response at 350 nm of (a) glass/STO and (b) glass/STO/TSE, where the TSE layer is a thin film of 5 layers of 4CzIPN/TP mixture after irradiation with a 375 nm pulse laser.

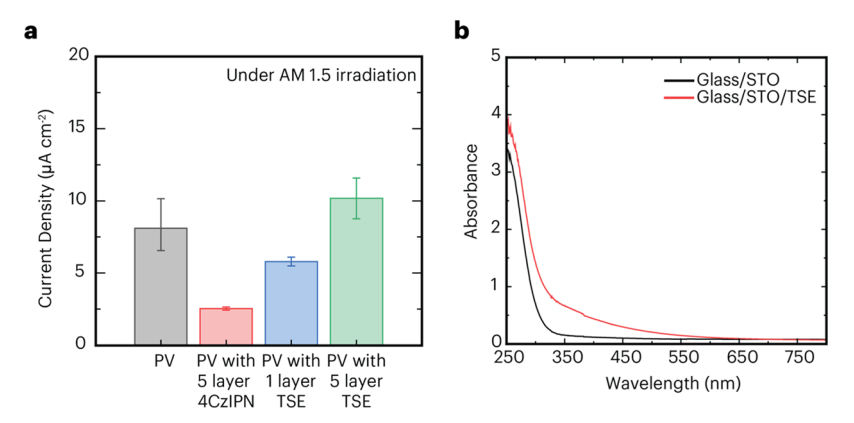


Figure 6. (a) J_{SC} value under an AM 1.5 solar simulator of the STO PV cell, the STO PV cell with 5 layers of deposited 4CzIPN, the STO PV cell with 1 layer of deposited TSE, and the STO PV cell with 5 layers of deposited TSE. (b) Absorbance of glass/STO and glass/STO/TSE, where the TSE layer is a thin film of 5 layers of 4CzIPN/TP mixture.

of TSE/STO. On the other hand, in the case of 4CzIPN alone on TiO_2 (Figure S5f, which means there is no STO in the device), the EQE/EQE₀ was larger than that of 4CzIPN on STO. Moreover, the data also showed that 4CzIPN is highly responsive to the light intensity. The high EQE/EQE₀ was probably due to the efficient charge separation in 4CzIPN and conduction to the conduction band edge of TiO_2 (at 4.4 eV), which is a deeper energy level than that of STO (at 3.75 eV). The case with 4CzIPN alone on TiO_2 is however not our focus, as our goal is to extract charge from STO. Overall, since 4CzIPN alone on STO did not show a significantly enhanced photocurrent, it is therefore confirmed that the large increase of the EQE in ITO/ $TiO_2/STO/TSE/PEDOT:PSS/Al$ would not occur when TTA-UC is not taking place.

Under UV light (Figure 4e), the EQE/EQE₀ value for TSE/STO PV cells exceeded that of the conventional PV cell only under intense light and with a thicker TSE layer. It is clear that UV light induces charge separation in STO of the conventional PV cell, particularly in $\lambda \leq 345$ nm. With low UV intensity (8 W cm⁻²), no photocurrent enhancement was observed in the TSE/STO PV cells with a single TSE layer, as compared with the conventional PV cells. It is noteworthy that the UV light source's spectrum (Figure S6) includes components with $\lambda > 345$ nm, which were partially transmitted through STO and absorbed by 4CzIPN. However, these components did not cause charge separation in 4CzIPN, i.e., electrons (or holes) in 4CzIPN's LUMO (or HOMO) did not transfer to STO's conduction band (or valence band) to add the source of photogenerated carriers. Even with a thicker TSE layer (in TSE/STO PV cells with 5-

layer TSE and intensity = 8 W cm⁻²), no enhancement in photocurrent was observed as the thicker TSE layer should have a higher light absorption. The only possible source for the observed EQE improvement was upconversion in the TSE layer. The EQE enhancement with the thicker TSE layer under highintensity UV light indicates that the photogeneration charge in STO is due to a higher upconversion quantum yield, with the TSE layer promoting the conduction of holes from STO's valence band to the HOMO of PEDOT:PSS (Figure 4f) through the HOMO level of TSE. It could also be said that the holes in TSE, generated after triplet-triplet energy transfer, might be conducted to PEDOT:PSS, while other holes from STO will replace it (by conduction from STO to TSE). To investigate charge transfer under illumination, we fabricated ITO/TiO₂/STO/TSE and performed KPFM measurement. As shown in Figure S7, the SPV value of the TSE surface on ITO/ TiO₂/STO/TSE was more negative. It means that the bulk TSE layer receives holes under illumination (both UV and visible light) from the underlying STO layer.

We also investigated the light responsiveness of TSE on STO from the time-resolved photoluminescence (TRPL) measurement. The STO/TSE thin film layer was fabricated on the glass substrate so that we see the direct PL response of TSE neighboring with STO. The TRPL response data (Figure 5) shows that TSE on STO was able to generate UV emission of 350 nm when irradiated with a longer wavelength (375 nm) pulse laser source. This observation implies that TSE, in the form of a solid thin film (after the evaporation of benzene), retains its ability to perform upconversion. This suggests that in

a thin film, the sensitizer and emitter molecules are in close proximity, facilitating the energy transfer required for TTA-UC even after the solvent has evaporated. Another possibility is that some benzene molecules might still be trapped in the thin film, contributing to stabilizing the triplet states.

Finally, the photocurrent performances of the STO PV, 4CzIPN/STO PV, and TSE/STO PV cells were compared (Figures 6 and S8) using the 1.5 AM solar simulator, and the result showed similar trends as the data shown in Figures 4 and S5. The enhancement of about 31% for the 5-layer TSE/STO PV cell compared to the STO PV cell clearly shows that solid-state upconversion occurred in the TSE/STO PV cells. It could also mean that the small $\Delta E_{\rm ST}$ value of 4CzIPN effectively promotes intersystem crossing for the TTA-UC process, instead of exciton diffusion and charge separation at the 4CzIPN/STO interface.

CONCLUSIONS

To conclude, this study demonstrates that integrating a triplet sensitizer-emitter (TSE) system with STO significantly enhances the external quantum efficiency (EQE) under visible light, particularly with 4CzIPN/TP as a thin film in the TSE/ STO PV cell, and further improvements are observed under a higher irradiance intensity. The thickness dependence of the TSE upconversion performance contributes to an increased efficiency without saturation in EQE/EQE₀, highlighting the potential of TSE/STO PV cells to utilize the high photon flux effectively. The efficiency outcomes might be enhanced by performing the sample preparation and measurements in an inert gas environment along with using an effective method to remove dissolved oxygen from the TSE solution. Regardless, the findings in this present study underscore the promising performance of using the TSE system as a thin film in PV cells for maximizing photon absorbance from a longer wavelength light source and reducing the parasitic light absorber.

■ EXPERIMENTAL SECTION

Main Chemicals. The sensitizer 4CzlPN (99.0%, Ossila), emitter QP (98.0%, TCI), emitter TP (99.0%, TCI), strontium nitrate (≥99.0%, Sigma-Aldrich), titanium diisopropoxide bis-(acetylacetonate) (75 wt % in isopropanol, Sigma-Aldrich), citric acid (≥99.5%, Sigma-Aldrich), ethylene glycol (99.8%, Sigma-Aldrich), Coumarin 6 (98%, Sigma-Aldrich), anatase TiO₂ (powder, Sigma-Aldrich), and PEDOT:PSS (Sigma-Aldrich, 3.0−4.0% in $\rm H_2O$) were used as received without any further purification.

Photoluminescence Response Measurement of the TSE **Solution.** The TSE solutions were prepared from the mixture of the sensitizer and emitter powders in benzene (concentration information is mentioned in the main text). A spectrophotometer (IHR 550, HORIBA) equipped with a CCD detector (Syncerity, HORIBA) was used for the measurement of the upconverted fluorescence intensity of the TSE solution. The intensity was measured in the wavelength range of 300-500 nm (average scan rate = 3 times; exposure time = 2 s; front entrance slit = 0.2 mm). A controlled volume (3 mL) of the TSE solution was placed in a UV transparent quartz cuvette (Scioutlet, 45 mm \times 12 mm \times 12 mm dimension). The 450 nm excitation LED light source (Figure S6, Chanzon, 50 W, 450 nm LED, fwhm = 15 nm) was connected to the power supply to adjust the excitation intensity. N2 gas was purged (N2 bubbling) into the TSE solution before PL measurement. The N₂ flow rate was set at 10 mL/min. The light irradiated the TSE solution in the cuvette, and then the upconverted fluorescence transmitted through the notch filter (Pixelteq, 2 mm thickness × 20 mm diameter) and reached the spectrophotometer. The notch filter allowed $\lambda \leq 400$ nm, for which the purpose was to filter the incident light (at the 450 nm spectrum). The upconverted fluorescence

of the TSE solution was around 350 nm, which is the wavelength having ${\sim}82.4\%$ transmittance through the notch filter.

Synthesis of the STO Precursor Solution by the Sol-Gel Method. The STO precursor solution was synthesized with adjustment from a previous study 43 and our previous study. 44 First, 3 mmol of strontium nitrate was dissolved in 5 mL of distilled water, obtaining a clear colorless solution. An equimolar amount of titanium diisopropoxide bis(acetylacetonate) was then added to form a milky, slightly orange solution. Next, 12 mmol of citric acid, dissolved in 10 mL of distilled water, was added to the mixture to promote homogeneity and the hydrolysis reaction. Additionally, 48 mmol of ethylene glycol was introduced to facilitate polymerization between the titanium ion and strontium nitrate. The molar ratio of titanium ions, citric acid, and ethylene glycol was set to 1:4:16. The molar ratio between citric acid and the strontium ion was adjusted to 4:1 to improve the homogeneity of the sol-gel network. The mixed precursor solution was heated at a constant 70 °C while being continuously stirred for 3 days, eventually forming a pale yellowish sol-gel STO precursor. The synthesized STO precursor gel was added to DMSO, creating a solution with a concentration of 3 g/mL.

Fabrication of the STO PV Cell (ITO/TiO₂/STO/PEDOT:PSS/ Al). The fabrication of STO PV Cell is based on our previous study on ITO/TiO₂/STO thin film. 44 Prepatterned ITO substrates (Zhuhai Kaivo, 20 mm \times 10 mm \times 1.1 mm of ITO on 20 mm \times 20 mm glass) were cleaned sequentially with soap, acetone, isopropyl alcohol, and ethanol in an ultrasonic bath and dried with a nitrogen purge. 100 μ L of anatase TiO2 dissolved in ethanol (1 g of TiO2 dissolved in 3 mL of ethanol) was dropped on the ITO surface for the spin-coating process (30 s of 200 rpm, followed by 30 s of 2000 rpm and 30 s of 5000 rpm). The TiO₂-coated ITO substrate was heated to 120 °C on the hot plate for 10 min. The TiO_2 layer was then heated at 550 °C in the quartz tube furnace for 30 min. After that, 100 μ L of the STO precursor solution was cast on the ITO/TiO₂ sample. The STO sol-gel precursor was used to fabricate the STO thin film, where a total of 20 layers of STO were coated in this step. The spin-coating step was initiated at 200 rpm for 30 s to evenly spread the solution over the substrate. Subsequently, the spin-coating step continued at 2000 rpm for 30 s, followed by spincoating at 5000 rpm for 30 s. The multilayer thin film was spin-coated on the substrate subsequently with the introduction of a drying process for each coated film layer. After each coated layer, a drying process was introduced to evaporate the solvent before the next solution was applied to prevent solvent trapping. To ensure DMSO evaporation, the thin film was dried on a hot plate at 180 °C for 15 min for each layer, as DMSO is not volatile in ambient conditions and has a boiling point of 189 °C. (Note: Drying over the boiling point of the solvent will cause the solvent to boil, resulting in bubble formation and destroying the uniformity of the thin film.) Once all of the multilayer thin film coatings were completed, the samples underwent annealing for 2 h at 300 °C in the tube furnace, followed by a heat treatment process for 2 h at 500 °C. Next, 50 µL of filtered PEDOT:PSS was coated on the ITO/TiO₂/ STO sample. PEDOT:PSS was filtered with a 0.45 μ m nylon filter (Whatman) prior to use. The PEDOT:PSS layer was heated at 120 °C on the hot plate for 30 min. Finally, an aluminum electrode was deposited on the PEDOT:PSS layer of the ITO/TiO2/STO/ PEDOT:PSS sample with a thermal evaporator (Auto 306, HHV). A 7 × 20 mm aluminum layer was deposited through a customized deposition mask during this process.

Fabrication of the TSE/Glass/STO PV Cell (TSE/Glass/ITO/TiO₂/STO/PEDOT:PSS/Al). A 3D-printed holder module designed for a printed circuit board (PCB) was created to hold the fabricated PV cell and to probe the anode and cathode electrodes (Figure S9). The cell holder's cap was designed with a 1 cm × 1 cm opening for incident light irradiance and for containing the TSE solution. The TSE mixtures were 50 μ M 4CzIPN:25 mM TP and 50 μ M 4CzIPN:300 μ M QP solutions. The choice of concentration is based on the previous study. ^{35,42} (Note that QP has a low solubility in benzene compared to those of TP and 4CzIPN.) 600 uL of the TSE solution was dropped on the glass side of ITO/TiO₂/STO/PEDOT:PSS/Al through the cell holder's 1 cm × 1 cm opening to form TSE/glass/ITO/TiO₂/STO/PEDOT:PSS/Al.

Fabrication of the TSE/STO PV Cell (ITO/TiO $_2$ /STO/TSE/PEDOT:PSS/Al). The fabrication process is similar to ITO/TiO $_2$ /STO/PEDOT:PSS/Al. But, the TSE solution (from 50 μ M 4CzIPN:25 mM TP in benzene solution) was deposited (30 s of 200 rpm, followed by 30 s of 2000 rpm and 30 s of 5000 rpm) before the PEDOT:PSS layer. The thin film was heated on the hot plate for 15 min at a temperature of 200 °C and then heated in the furnace for 30 min at 400 °C to evaporate the residual solvent.

Thin Film Thickness Measurement. The thickness of the spin-coated thin film was measured using a profilometry machine (DektakXT, Bruker). To determine the film thickness, a portion of the coated surface was carefully removed by applying a mechanical force with a blade, exposing the underlying substrate region. The film thickness was then measured by calculating the difference between the original coated surface and the newly exposed surface.

Kelvin Probe Force Microscopy Measurement. The Kelvin probe force microscopy (KPFM) mode was used from an AFM (Park Systems NX-10) with noncontact mode cantilevers (NSC36_B/Pt, Park Systems). The scanning rate was set to be 0.5 Hz with a scan area of $10 \, \mu \text{m} \times 10 \, \mu \text{m}$. For the KPFM mode, the cantilever tips were set 50 nm from the sample. The profile of the light source is shown in Figure S6. The surface topology images and the SKPM images were obtained and analyzed using XEI software, which is an image processing program for scanning probe microscopy data developed by Park Systems.

Time-Resolved Photoluminescence (TRPL) Measurement. A spectrometer (FLS920, Edinburgh Instrument), equipped with a 375 nm pulsed laser, was used to measure the photoluminescence response of the thin film samples, which are glass/STO/TSE and glass/STO. These thin film samples were fabricated by spin-coating onto microslide glass, a process similar to that used for the TSE/STO PV samples but without additional layers.

PV Performance Measurement. The PV cells were mounted on the holder module (Figure S9). The I-V characteristics of the PV cell were measured using a source measure unit (SMU 2450, Keithley) under the irradiance of 450 nm visible light (Chanzon), 345 nm UV light (Marktech), and solar AM 1.5. To simulate average AM 1.5 solar irradiance, a solar simulator (LS1000, Solar Light Company), controlled by its xenon light power supply (XPS-1600, Solar Light Company), was used. With a pyranometer (PMA2144, Solar Light Company), the solar light was adjusted to 1000 W/m^2 , simulating average solar irradiance.

ASSOCIATED CONTENT

Solution Supporting Information

The Supporting Information is available free of charge at https://pubs.acs.org/doi/10.1021/acsaem.3c02971.

Light source intensity-dependent and concentration-dependent PL spectra of TSE pairs; additional EQE data for several PV cells; light source profile; KPFM data for ITO/TiO₂/STO/TSE; *I*–*V* curve data for TSE/STO PV cells; the image of the PV cell holder module; and experimental details on quantum yield measurement (PDF)

AUTHOR INFORMATION

Corresponding Author

M. Fairus Ahmad — Faculty of Electronic Engineering & Technology, Universiti Malaysia Perlis, 02600 Arau, Perlis, Malaysia; Institute of Nano Electronic Engineering, Universiti Malaysia Perlis, 02600 Arau, Perlis, Malaysia; occid.org/0000-0002-2734-8176; Email: fairusahmad@unimap.edu.my

Authors

Kelvin V. Y. Jie — Faculty of Electronic Engineering & Technology, Universiti Malaysia Perlis, 02600 Arau, Perlis, Malaysia; orcid.org/0009-0004-3060-649X

- A. Rahman Mohmad Institute of Microengineering and Nanoelectronics, Universiti Kebangsaan Malaysia, 43600 Bangi, Selangor, Malaysia
- A. Mawardi Ismail Faculty of Electronic Engineering & Technology, Universiti Malaysia Perlis, 02600 Arau, Perlis, Malaysia
- M. Natashah Norizan Faculty of Electronic Engineering & Technology, Universiti Malaysia Perlis, 02600 Arau, Perlis, Malaysia; orcid.org/0000-0002-2198-1077
- M. Mahyiddin Ramli Faculty of Electronic Engineering & Technology, Universiti Malaysia Perlis, 02600 Arau, Perlis, Malaysia; Institute of Nano Electronic Engineering, Universiti Malaysia Perlis, 02600 Arau, Perlis, Malaysia
- Safizan Shaari Faculty of Electronic Engineering & Technology, Universiti Malaysia Perlis, 02600 Arau, Perlis, Malaysia
- Yusran Sulaiman Department of Chemistry, Faculty of Science, Universiti Putra Malaysia, 43400 UPM Serdang, Selangor, Malaysia; Functional Devices Laboratory, Institute of Advanced Technology, Universiti Putra Malaysia, 43400 UPM Serdang, Selangor, Malaysia; orcid.org/0000-0002-1841-2447
- Shamsul A. A. Rais Faculty of Electronic Engineering & Technology, Universiti Malaysia Perlis, 02600 Arau, Perlis, Malaysia
- Shazlina Johari Faculty of Electronic Engineering & Technology, Universiti Malaysia Perlis, 02600 Arau, Perlis, Malaysia

Complete contact information is available at: https://pubs.acs.org/10.1021/acsaem.3c02971

Author Contributions

This manuscript was written through contributions from all authors. All authors have given approval to the final version of the manuscript. Supervision and conceptualization: M.F.A.; conducting the experiments: K.V.Y.J. and A.R.M.; writing and validation: K.V.Y.J. and M.F.A.; and review and editing: M.F.A., K.V.Y.J., A.R.M., A.M.I., M.N.N., M.M.R., S.S., Y.S., S.A.A.R., and S.J.

Notes

The authors declare no competing financial interest.

ACKNOWLEDGMENTS

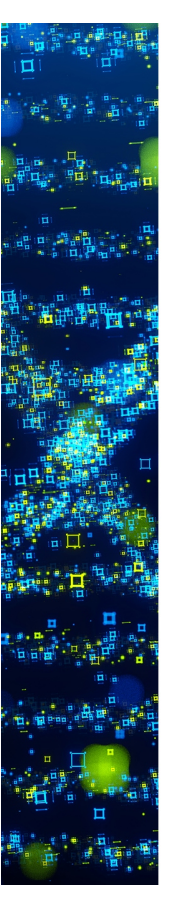
The authors express their gratitude to the Faculty of Electronic Engineering & Technology at Universiti Malaysia Perlis and the Ministry of Higher Education Malaysia for the financial support provided through the Fundamental Research Grant Scheme (No. FRGS/1/2021/TK0/UNIMAP/02/58). Special acknowledgment is due to Prof. Dr. Prabakaran Poopalan for the valuable assistance in the photoluminescence measurement setup. The authors also extend their appreciation to Bahari Man, Mohd Husyaidi, and M. Nazrul Zahari for their help with microscopy-related measurements. Last, the authors are thankful to the Centre of Excellence for Renewable Energy -CERE, Universiti Malaysia Perlis and the Institute of Microengineering and Nanoelectronics, Universiti Kebangsaan Malaysia for granting permission to use their equipment. The authors would like to acknowledge the "beam" illustration designed by Freepik for the use in TOC, Figure 2, Figure 3, and Figure 4.

REFERENCES

- (1) Lewis, N. S. Toward Cost-Effective Solar Energy Use. *Science* **2007**, 315 (5813), 798–801.
- (2) Schulze, T. F.; Czolk, J.; Cheng, Y.-Y.; Fückel, B.; MacQueen, R. W.; Khoury, T.; Crossley, M. J.; Stannowski, B.; Lips, K.; Lemmer, U.; Colsmann, A.; Schmidt, T. W. Efficiency Enhancement of Organic and Thin-Film Silicon Solar Cells with Photochemical Upconversion. *J. Phys. Chem. C* 2012, 116 (43), 22794–22801.
- (3) Bati, A. S. R.; Zhong, Y. L.; Burn, P. L.; Nazeeruddin, M. K.; Shaw, P. E.; Batmunkh, M. Next-Generation Applications for Integrated Perovskite Solar Cells. *Commun. Mater.* **2023**, *4* (1), 2.
- (4) Jagadamma, L. K.; Wang, S. Wide-Bandgap Halide Perovskites for Indoor Photovoltaics. *Front Chem.* **2021**, *9*, 632021.
- (5) Roy, P.; Ghosh, A.; Barclay, F.; Khare, A.; Cuce, E. Perovskite Solar Cells: A Review of the Recent Advances. *Coatings* **2022**, *12* (8), 1089.
- (6) Castelletto, S.; Boretti, A. Luminescence Solar Concentrators: A Technology Update. *Nano Energy* **2023**, *109*, No. 108269.
- (7) Baiju, A.; Yarema, M. Status and Challenges of Multi-Junction Solar Cell Technology. Front. Energy Res. 2022, 10, 971918.
- (8) Zhou, Y.; Li, X.; Lin, H. To Be Higher and Stronger—Metal Oxide Electron Transport Materials for Perovskite Solar Cells. *Small* **2020**, *16* (15), No. 1902579.
- (9) Goetz, S.; Mehanni, D.; Bansal, N.; Kubicek, B.; Wibowo, R. A.; Bauch, M.; Linke, C.; Franzke, E.; Winkler, J.; Meyer, T.; Narbey, S.; Stock, D.; Valtiner, M.; Dimopoulos, T. Low-Temperature-Processed Transparent Electrodes Based on Compact and Mesoporous Titanium Oxide Layers for Flexible Perovskite Solar Cells. *ACS Appl. Energy Mater.* **2022**, *5* (5), 5318–5330.
- (10) Nguyen, D. C. T.; Park, H.; Woo, H. Y.; Kim, S.; Lee, S.-H. Inorganic/Organic Electron Transport Interface Engineering for Planar and Fiber-Shaped Organic Solar Cells. *ACS Appl. Energy Mater.* **2023**, *6* (14), 7509–7520.
- (11) Latypova, A. F.; Emelianov, N. A.; Balakirev, D. O.; Sukhorukova, P. K.; Kalinichenko, N. K.; Kuznetsov, P. M.; Luponosov, Y. N.; Aldoshin, S. M.; Ponomarenko, S. A.; Troshin, P. A.; Frolova, L. A. Design Principles for Organic Small Molecule Hole-Transport Materials for Perovskite Solar Cells: Film Morphology Matters. ACS Appl. Energy Mater. 2022, 5 (5), 5395–5403.
- (12) Dahiya, H.; Suthar, R.; Khandelwal, K.; Karak, S.; Sharma, G. D. Recent Advances in Organic and Inorganic Hole and Electron Transport Layers for Organic Solar Cells: Basic Concept and Device Performance. ACS Appl. Electron Mater. 2022, 4 (11), 5119–5143.
- (13) Shen, Y.; Deng, K.; Li, L. Spiro-OMeTAD-Based Hole Transport Layer Engineering toward Stable Perovskite Solar Cells. *Small Methods* **2022**, *6* (11), No. 2200757.
- (14) Yao, Y.; Cheng, C.; Zhang, C.; Hu, H.; Wang, K.; De Wolf, S. Organic Hole-Transport Layers for Efficient, Stable, and Scalable Inverted Perovskite Solar Cells. *Adv. Mater.* **2022**, 34 (44), No. 2203794.
- (15) Zhang, X.; Zhang, H.; Li, Y.; Zafar, S.; Yang, S.; Chen, J.; Zhou, H.; Zhang, Y. Recent Progress in Hole-Transporting Layers of Conventional Organic Solar Cells with p—i—n Structure. *Adv. Funct Mater.* **2022**, 32 (44), No. 2205398.
- (16) Fujiwara, H.; Nakane, A.; Murata, D.; Tampo, H.; Matsui, T.; Shibata, H. *Analysis of Optical and Recombination Losses in Solar Cells*; Springer, 2018; Vol. 2, pp 29–82.
- (17) Morawiec, S.; Holovský, J.; Mendes, M. J.; Müller, M.; Ganzerová, K.; Vetushka, A.; Ledinský, M.; Priolo, F.; Fejfar, A.; Crupi, I. Experimental Quantification of Useful and Parasitic Absorption of Light in Plasmon-Enhanced Thin Silicon Films for Solar Cells Application. Sci. Rep. 2016, 6 (1), No. 22481.
- (18) Takata, T.; Jiang, J.; Sakata, Y.; Nakabayashi, M.; Shibata, N.; Nandal, V.; Seki, K.; Hisatomi, T.; Domen, K. Photocatalytic Water Splitting with a Quantum Efficiency of Almost Unity. *Nature* **2020**, *581* (7809), 411–414.
- (19) Koshi, N. A.; Murthy, D. H. K.; Chakraborty, S.; Lee, S.-C.; Bhattacharjee, S. Probing Photoexcited Charge Carrier Trapping and

- Defect Formation in Synergistic Doping of SrTiO₃. ACS Appl. Energy Mater. **2022**, 5 (1), 1159–1168.
- (20) Avcıoğlu, C.; Avcıoğlu, S.; Bekheet, M. F.; Gurlo, A. Photocatalytic Overall Water Splitting by SrTiO₃: Progress Report and Design Strategies. *ACS Appl. Energy Mater.* **2023**, *6* (3), 1134–1154.
- (21) Felter, K. M.; Fravventura, M. C.; Koster, E.; Abellon, R. D.; Savenije, T. J.; Grozema, F. C. Solid-State Infrared Upconversion in Perylene Diimides Followed by Direct Electron Injection. *ACS Energy Lett.* **2020**, *5* (1), 124–129.
- (22) Hanna, M. C.; Nozik, A. J. Solar Conversion Efficiency of Photovoltaic and Photoelectrolysis Cells with Carrier Multiplication Absorbers. *J. Appl. Phys.* **2006**, *100* (7), 074510.
- (23) Li, J.; Tang, X.-G.; Liu, Q.-X.; Jiang, Y.-P.; Li, W.-H. Enhancement of the Photoelectric Properties of Composite Oxide TiO2-SrTiO3 Thin Films. *Adv. Compos. Hybrid Mater.* **2022**, 5 (2), 1557–1565.
- (24) Neophytou, M.; De Bastiani, M.; Gasparini, N.; Aydin, E.; Ugur, E.; Seitkhan, A.; Moruzzi, F.; Choaie, Y.; Ramadan, A. J.; Troughton, J. R.; Hallani, R.; Savva, A.; Tsetseris, L.; Inal, S.; Baran, D.; Laquai, F.; Anthopoulos, T. D.; Snaith, H. J.; De Wolf, S.; McCulloch, I. Enhancing the Charge Extraction and Stability of Perovskite Solar Cells Using Strontium Titanate (SrTiO 3) Electron Transport Layer. ACS Appl. Energy Mater. 2019, 2 (11), 8090–8097.
- (25) Richards, B. S.; Hudry, D.; Busko, D.; Turshatov, A.; Howard, I. A. Photon Upconversion for Photovoltaics and Photocatalysis: A Critical Review. *Chem. Rev.* **2021**, *121* (15), 9165–9195.
- (26) Carrod, A. J.; Gray, V.; Börjesson, K. Recent Advances in Triplet—Triplet Annihilation Upconversion and Singlet Fission, towards Solar Energy Applications. *Energy Environ. Sci.* **2022**, *15* (12), 4982—5016.
- (27) Dziobek-Garrett, R.; Imperiale, C. J.; Wilson, M. W. B.; Kempa, T. J. Photon Upconversion in a Vapor Deposited 2D Inorganic—Organic Semiconductor Heterostructure. *Nano Lett.* **2023**, 23 (11), 4837–4843.
- (28) Naimovičius, L.; Bharmoria, P.; Moth-Poulsen, K. Triplet—Triplet Annihilation Mediated Photon Upconversion Solar Energy Systems. *Mater. Chem. Front* **2023**, *7* (12), 2297–2315.
- (29) Morifuji, T.; Takekuma, Y.; Nagata, M. Integrated Photon Upconversion Dye-Sensitized Solar Cell by Co-Adsorption with Derivative of Pt-Porphyrin and Anthracene on Mesoporous TiO₂. ACS Omega **2019**, 4 (6), 11271–11275.
- (30) de Wild, J.; Meijerink, A.; Rath, J. K.; van Sark, W. G. J. H. M.; Schropp, R. E. I. Upconverter Solar Cells: Materials and Applications. *Energy Environ. Sci.* **2011**, *4* (12), 4835.
- (31) Goldschmidt, J. C.; Fischer, S. Upconversion for Photovoltaics a Review of Materials, Devices and Concepts for Performance Enhancement. *Adv. Opt Mater.* **2015**, 3 (4), 510–535.
- (32) Zhou, Y.; Ruchlin, C.; Robb, A. J.; Hanson, K. Singlet Sensitization-Enhanced Upconversion Solar Cells via Self-Assembled Trilayers. ACS Energy Lett. 2019, 4 (6), 1458–1463.
- (33) Beery, D.; Wheeler, J. P.; Arcidiacono, A.; Hanson, K. CdSe Quantum Dot Sensitized Molecular Photon Upconversion Solar Cells. *ACS Appl. Energy Mater.* **2020**, 3 (1), 29–37.
- (34) Schoenauer Sebag, M.; Hu, Z.; de Oliveira Lima, K.; Xiang, H.; Gredin, P.; Mortier, M.; Billot, L.; Aigouy, L.; Chen, Z. Microscopic Evidence of Upconversion-Induced Near-Infrared Light Harvest in Hybrid Perovskite Solar Cells. *ACS Appl. Energy Mater.* **2018**, *1* (8), 3537–3543.
- (35) Yanai, N.; Kozue, M.; Amemori, S.; Kabe, R.; Adachi, C.; Kimizuka, N. Increased Vis-to-UV Upconversion Performance by Energy Level Matching between a TADF Donor and High Triplet Energy Acceptors. *J. Mater. Chem. C Mater.* **2016**, *4* (27), 6447–6451.
- (36) Singh-Rachford, T. N.; Castellano, F. N. Low Power Visible-to-UV Upconversion. *J. Phys. Chem. A* **2009**, *113* (20), 5912–5917.
- (37) Lee, H. L.; Lee, M. S.; Park, H.; Han, W. S.; Kim, J. H. Visible-to-UV Triplet-Triplet Annihilation Upconversion from a Thermally Activated Delayed Fluorescence/Pyrene Pair in an Air-Saturated Solution. *Korean J. Chem. Eng.* **2019**, *36* (11), 1791–1798.

- (38) Murakami, Y.; Motooka, A.; Enomoto, R.; Niimi, K.; Kaiho, A.; Kiyoyanagi, N. Visible-to-Ultraviolet (<340 Nm) Photon Upconversion by Triplet—Triplet Annihilation in Solvents. *Phys. Chem. Chem. Phys.* **2020**, 22 (46), 27134—27143.
- (39) Bharmoria, P.; Bildirir, H.; Moth-Poulsen, K. Triplet—Triplet Annihilation Based near Infrared to Visible Molecular Photon Upconversion. *Chem. Soc. Rev.* **2020**, *49* (18), 6529–6554.
- (40) Ahmad, M. F.; Suzuki, M.; Abe, T.; Nagai, K. Enhanced Oxidation Power in Photoelectrocatalysis Based on a Micrometer-Localized Positive Potential in a Terrace Hetero p—n Junction. NPG Asia Mater. 2018, 10 (7), 630.
- (41) Caprioglio, P.; Stolterfoht, M.; Wolff, C. M.; Unold, T.; Rech, B.; Albrecht, S.; Neher, D. On the Relation between the Open-Circuit Voltage and Quasi-Fermi Level Splitting in Efficient Perovskite Solar Cells. *Adv. Energy Mater.* **2019**, *9* (33), No. 1901631.
- (42) Yurash, B.; Dixon, A.; Espinoza, C.; Mikhailovsky, A.; Chae, S.; Nakanotani, H.; Adachi, C.; Nguyen, T. Efficiency of Thermally Activated Delayed Fluorescence Sensitized Triplet Upconversion Doubled in Three-Component System. *Adv. Mater.* **2022**, *34* (5), 2103976.
- (43) Neophytou, M.; Bastiani, M. De.; Gasparini, N.; Aydin, E.; Ugur, E.; Seitkhan, A.; Moruzzi, F.; Choaie, Y.; Ramadan, A. J.; Troughton, J. R.; Hallani, R.; Savva, A.; Tsetseris, L.; Inal, S.; Baran, D.; Laquai, F.; Anthopoulos, T. D.; Snaith, H. J.; Wolf, S. De.; McCulloch, I. Enhancing the Charge Extraction and Stability of Perovskite Solar Cells Using Strontium Titanate (SrTiO 3) Electron Transport Layer. ACS Appl. Energy Mater. 2019, 2 (11), 8090–8097.
- (44) Jie, K. V. Y.; Ahmad, M. F.; Ramli, M. M.; Shaari, S.; Ismail, A. M.; Sulaiman, Y. Fabrication of Strontium Titanate Thin Film with Precrystallized Layer via Sol-Gel Spin Coating Method. *International Journal of Nanoelectronics and Materials* **2022**, *15*, 331–339.



CAS BIOFINDER DISCOVERY PLATFORM™

STOP DIGGING THROUGH DATA —START MAKING DISCOVERIES

CAS BioFinder helps you find the right biological insights in seconds

Start your search

